INORGANIC CHEMISTRY
FRONTIERS

RESEARCH ARTICLE

View Article Online
View Journal | View Issue

Cite this: *Inorg. Chem. Front.*, 2024, **11**, 6486

Enantioselective assembly of tetrahedral $Zr_4(embonate)_6$ cages in zeolitic frameworks for synergetic circularly polarized luminescence†

Xin Meng,[a,b] Qing-Rong Ding,[a] Shu-Mei Chen,[b] Yan-Ping He *[a] and Jian Zhang *[a]

Received 28th June 2024,
Accepted 7th August 2024

DOI: 10.1039/d4qi01624f

rsc.li/frontiers-inorganic

Herein the chiral resolution of racemic Zr_4L_6 tetrahedral cages has been realized using luminescent enantiopure coordination cations. Accordingly, anionic ΔΔΔΔ-Zr_4L_6 and ΛΛΛΛ-Zr_4L_6 cages (L = embonate) were completely resolved using enantiopure $[Ag(R\text{-BINAP})_2]^+$ and $[Ag(S\text{-BINAP})_2]^+$ cations, respectively, and a pair of pure enantiomers (**PTC-374(*R*,Δ)** and **PTC-374(*S*,Λ)**; PTC = polynuclear titanium cage) were easily prepared and structurally well-characterized, featuring an uncommon cage-supported supramolecular framework with zeolitic SOD topology. The stepwise transfer of homochirality can be clearly observed in the unusual resolution process. Moreover, the perfect combination of two functional components endows such co-assembled materials with synergistic circular dichroism performance, enhanced fluorescence and circularly polarized luminescence response.

1. Introduction

Because of its highly directional and highly spatiotemporal resolution, circularly polarized luminescence (CPL) has broad application prospects in optical displays, biological imaging and sensing, information storage and processing, photoelectric devices, *etc.*[1–4] In order to achieve practical applications in chiral photonics and electronics, numerous elaborately designed materials have been developed for CPL,[5–13] and a lot of effort has been directed toward adjusting and improving luminescence quantum yield, the dissymmetric factor, g_{lum}, and so on.[14–20] As we all know, CPL reflecting chirality in the excited states of materials requires bright luminescence and sufficiently strong chiral signals for measurement. Thus, the purposeful combination of the above two functional components would be an interesting topic.

In recent years, our group has been devoted to research work based on the anionic Ti_4L_6 or Zr_4L_6 cage (L = embonate).[21] This cage features abundant interaction sites (uncoordinated carboxyl oxygen atoms and naphthyls), and high solubility and stability in common solvents, and turns out to be an excellent building block for further assembly.[22–28] Similar to other tetrahedral M_4L_6 cages constructed from achiral bidentate ligands and octahedral metal ions, the Ti_4L_6 or Zr_4L_6 cage also forms an intrinsically chiral structure with all metal centers having the same chiral configuration (Δ or Λ). However, such M_4L_6 cages usually exist as racemic mixtures in solution or in the solid state, which limits their applications. Fortunately, we have achieved the chiral resolution of Ti_4L_6 cages with enantiopure $[Mn(DCH)_3]^{2+}$ or $[Ag_4(DCH)_5]^{4+}$ units (DCH = 1*R*,2*R*-(−)- or (1*S*,2*S*)-(+)-1,2-diaminocyclohexane), and discovered that the separated homochiral Ti_4L_6 cage shows multiple strong CD peaks.[29,30] Thus, a simple idea is to combine two structural types (*e.g.* the Ti_4L_6 or Zr_4L_6 cage and a strong luminescence unit) into one system, which may be a new construction mode for CPL materials.

[a]*State Key Laboratory of Structural Chemistry, Fujian Institute of Research on the Structure of Matter, Chinese Academy of Sciences, Fuzhou, Fujian 350002, P. R. China. E-mail: hyp041@163.com, zhj@fjirsm.ac.cn*
[b]*College of Chemistry, Fuzhou University, Fuzhou, Fujian 350108, China*

†Electronic supplementary information (ESI) available: Additional experimental details, crystallographic studies, additional figures, and general characterization. CCDC 2356638–2356641. For ESI and crystallographic data in CIF or other electronic format see DOI: https://doi.org/10.1039/d4qi01624f

Jian Zhang

Jian Zhang: We are honored to present a paper in the themed collection celebrating the 10th anniversary of Inorganic Chemistry Frontiers. *This journal has greatly promoted the development of the inorganic chemistry discipline. We have witnessed the success of the journal over the past decade, and wish it to be a top journal in this field.*

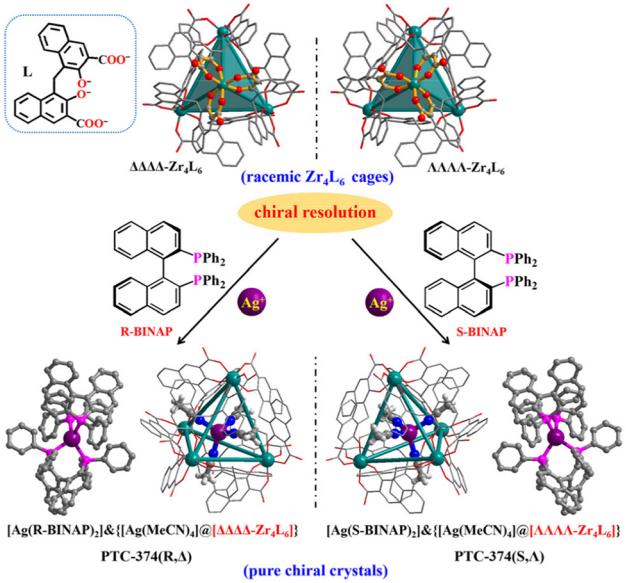

Fig. 1 Synthetic optical resolution of racemic Zr_4L_6 cages and crystal structures of **PTC-374(*R*,Δ)** and **PTC-374(*S*,Λ)** enantiomers. Most H atoms have been removed for clarity. Atom color code: purple, Ag; olive, Zr; pink, P; red, O; gray, C; off white, H.

From the above considerations, herein we have realized the chiral resolution of Zr_4L_6 cages using luminescent enantiopure coordination cations, and studied the synergistic CPL property. Through our methodology, the anionic ΔΔΔΔ-Zr_4L_6 and ΛΛΛΛ-Zr_4L_6 cages can be completely resolved with π-conjugated enantiopure $[Ag(R\text{-BINAP})_2]^+$ and $[Ag(S\text{-BINAP})_2]^+$ cations (*R*/*S*-BINAP = (*R*)/(*S*)-2,2′-bis(diphenylphosphino)-1,1′-binaphthyl), respectively (Fig. 1). Consequently, ΔΔΔΔ-Zr_4L_6 and $[Ag(R\text{-BINAP})_2]^+$ or ΛΛΛΛ-Zr_4L_6 and $[Ag(S\text{-BINAP})_2]^+$ are tactfully bonded, giving rise to a pair of pure enantiomers (**PTC-374(*R*,Δ)** and **PTC-374(*S*,Λ)**). Remarkably, **PTC-374(*R*,Δ)** (or **PTC-374(*S*,Λ)**) exhibits an uncommon cage-supported supramolecular framework with zeolitic SOD topology. By the formation of an ordered co-assembled material, its comprehensive performance, including circular dichroism (CD) and fluorescence, can be further improved, thus demonstrating CPL enhancement.

2. Experimental

Synthesis of $(Me_2NH_2)_{5.5}[Ag(MeCN)_4]\cdot\{[Ag(R\text{-BINAP})_2]_{1.5}(\Delta\Delta\Delta\Delta\text{-}Zr_4L_6)\}\cdot$guests (PTC-374(*R*,Δ))

The above pre-synthesized PTC-101(Δ,Λ) was used as the Zr_4L_6 cage raw material. PTC-101(Δ,Λ) (40 mg, 0.01 mmol), Ag(CH_3COO) (10 mg, 0.06 mmol) and (*R*)-(+)-2,2′-bis(diphenylphosphino)-1,1′-binaphthyl (*R*-BINAP, 30 mg, 0.05 mmol) were dissolved in 3 mL of DMSO/MeCN/H_2O (0.5 : 2 : 0.5, v/v, DMSO = dimethyl sulfoxide) mixed solvent, and then the solution was sealed in a 20 mL vial. The mixture was heated at 80 °C for 3 days. After being cooled to room temperature, yellowish crystals of **PTC-374(*R*,Δ)** were obtained (yield: 30% based on PTC-101(Δ,Λ)).

Synthesis of $(Me_2NH_2)_{5.5}[Ag(MeCN)_4]\cdot\{[Ag(S\text{-BINAP})_2]_{1.5}(\Lambda\Lambda\Lambda\Lambda\text{-}Zr_4L_6)\}\cdot$guests (PTC-374(S,Λ))

This compound was synthesized by substituting *R*-BINAP with (*S*)-(−)-2,2′-bis(diphenylphosphino)-1,1′-binaphthyl (*S*-BINAP) in the above synthetic procedure for **PTC-374(*R*,Δ)**.

Synthesis of $[Ag(R\text{-BINAP})_2](ClO_4)\cdot$guests (*R*-Ag)

R-BINAP (30 mg, 0.05 mmol) and $AgClO_4$ (15 mg, 0.07 mmol) were dissolved in 3 mL of DMF/EtOH/H_2O (1 : 1 : 1, v/v) mixed solvent, and then the solution was sealed in a 10 mL vial. The mixture was heated at 80 °C for 3 days. After being cooled to room temperature, clear crystals of ***R*-Ag** were obtained (yield: 50% based on *R*-BINAP).

Synthesis of $[Ag(S\text{-BINAP})_2](ClO_4)\cdot$guest (*S*-Ag)

This compound was synthesized by substituting *R*-BINAP with *S*-BINAP in the above synthetic procedure for ***S*-Ag**.

3. Results and discussion

Solvothermal self-assembly of $Zr(OPr)_4$ or $ZrCl_4$ with emonic acid (H_4L) gives rise to anionic tetrahedral Zr_4L_6 cages in orthorhombic (PTC-101(Δ,Λ)) or cubic (PTC-102(Δ) and PTC-102(Λ)) supramolecular arrangements (Fig. S1 and S2†), which has been successfully demonstrated in our previous work.[21] Although the Zr_4L_6 cage is chiral, both ΔΔΔΔ-Zr_4L_6 and ΛΛΛΛ-Zr_4L_6 isomers exist in the achiral crystal structure of PTC-101(Δ,Λ). Although spontaneous resolution can separate ΔΔΔΔ-Zr_4L_6 and ΛΛΛΛ-Zr_4L_6 cages into single crystals (PTC-102(Δ) and PTC-102(Λ)), the bulk sample is a conglomerate with an equal mixture of crystals of opposite handedness. To obtain homochiral samples for CPL study, PTC-101(Δ,Λ) with high yield was selected to carry out the optical resolution of Zr_4L_6 cages in this work. Large π-conjugated chiral organic ligands *R*/*S*-BINAP were introduced into the assembled system. Accordingly, *R*/*S*-BINAP and Ag^+ ions were dissolved in the DMSO/MeCN/H_2O solution of PTC-101(Δ,Λ) for resolution (Fig. S3†), and orange dodecahedral crystals of **PTC-374(*R*,Δ)** and **PTC-374(*S*,Λ)** were obtained, respectively. In addition, the chiral enantiomers of ***R*-Ag** and ***S*-Ag** were also prepared using *R*/*S*-BINAP and Ag^+ ions in DMF/EtOH/H_2O (Fig. S4†).

Single-crystal X-ray diffraction analysis revealed that both **PTC-374(*R*,Δ)** and **PTC-374(*S*,Λ)** crystallized in the cubic chiral space group *I*23 (Table S1†). Their asymmetric unit contained one-third of a formula unit (Fig. S5 and S6†). Only the detailed structure of **PTC-374(*S*,Λ)** will be described here. As shown in Fig. 1, the Ag(I) center is P,P-chelated by two *S*-BINAP ligands, generating a cationic $[Ag(S\text{-BINAP})_2]^+$ ion. Interestingly, each $[Ag(S\text{-BINAP})_2]^+$ ion is connected to four adjacent $[Ag(S\text{-BINAP})_2]^+$ ions through rich C–H···π interactions. When each cation is treated as a node, the 3D supramolecular framework can be simplified into a zeolite-type SOD topology, and it has

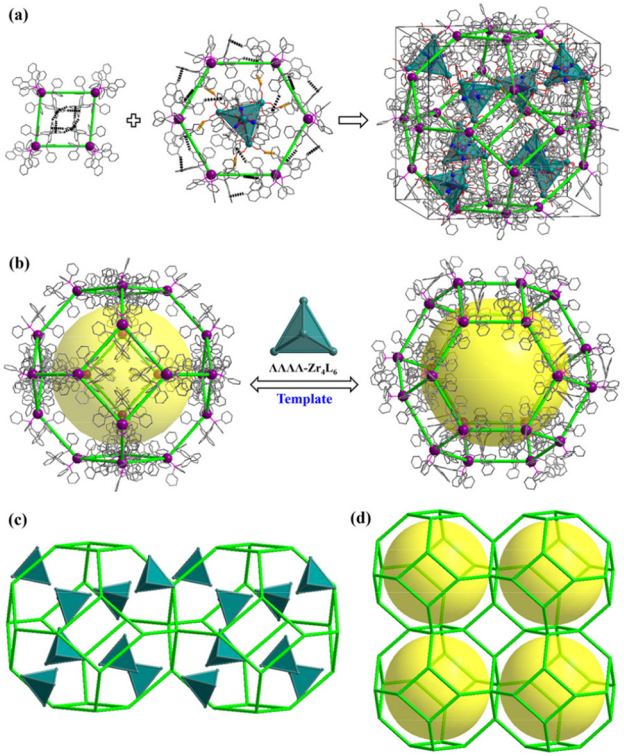

Fig. 2 Packing structure of **PTC-374(*S*,Λ)**: (a and b) formation of ΛΛΛΛ-Zr_4L_6 cage-supported zeolite SOD-type supramolecular framework and its simplified topology network (c and d).

the basic composite building unit of the SOD cage (Fig. 2). Each SOD cage has six square faces and eight hexagonal faces, which are all shared with neighboring cages. Tactfully, ΛΛΛΛ-Zr_4L_6 cages are located at the centroid of each hexagonal face, which further stabilize the whole architecture *via* C–H···O hydrogen bonds and C–H···π interactions (Fig. 2a and S7†). Unexpectedly, an *in situ* formed $[Ag(MeCN)_4]^+$ cation is found in each ΛΛΛΛ-Zr_4L_6 cage, which is accommodated within the cage through the C–H···π interactions, reflecting its suitable size and shape complementarity for such a tetrahedral cavity. Thus, an interesting host–guest $\{[Ag(MeCN)_4]@[ΛΛΛΛ\text{-}Zr_4L_6]\}^{7-}$ cage is obtained. Here, perfect matching between anionic ΛΛΛΛ-Zr_4L_6 cages and $[Ag(S\text{-BINAP})_2]^+$ cations can also be observed in **PTC-374(*S*,Λ)**. With suitable supramolecular interactions such as C–H···π and C–H···O (Fig. 2a and S7†), the ΛΛΛΛ-Zr_4L_6 cage is confined to the hexagonal face of the SOD cage. In other words, with the anionic ΛΛΛΛ-Zr_4L_6 cage as the support template, $[Ag(S\text{-BINAP})_2]^+$ cations are stacked into a regular supramolecular framework through suitable C–H···π interactions. In short, charge-driven and H-bonding-driven co-assembly of anionic Zr_4L_6 cages and $[Ag(R\text{-BINAP})_2]^+$ cations results in an ordered supramolecular framework with zeolitic SOD topology (Fig. 2b and c). The combination of cage and cation may render synergetic properties that cannot be achieved using a single component.

As expected, the opposite $[Ag(R\text{-BINAP})_2]^+$ units and ΔΔΔΔ-Zr_4L_6 cages as well as the opposite H-bonded framework can be observed in **PTC-374(*R*,Δ)**. Obviously, the stepwise transfer of homochirality is presented in the resolution process. The origin of the achieved homochirality is from the enantiopure ligand (*R*-BINAP or *S*-BINAP) and the related coordination cation ($[Ag(R\text{-BINAP})_2]^+$ or $[Ag(S\text{-BINAP})_2]^+$). Next, the $[Ag(R\text{-BINAP})_2]^+$ (or $[Ag(S\text{-BINAP})_2]^+$) cations demonstrated their enantioselectivity towards anionic Zr_4L_6 cages through suitable H-bonding interactions, achieving successful resolution that led to a homochiral structure with only ΔΔΔΔ-Zr_4L_6 isomers in **PTC-374(*R*,Δ)** or ΛΛΛΛ-Zr_4L_6 isomers in **PTC-374(*S*,Λ)**. For the convenience of comparison, the chiral enantiomers of ***R*-Ag** and ***S*-Ag** have also been provided (Fig. S8–10†), which are composed of $[Ag(R\text{-BINAP})_2]^+$ and $[Ag(S\text{-BINAP})_2]^+$ cations with $[ClO_4]^-$ counter anions, respectively. The mirror images can also be observed in the chiral structures of ***R*-Ag** and ***S*-Ag** (Fig. S11†).

SEM and electron spectroscopy analyses of **PTC-374(*S*,Λ)** show that P, Ag and Zr atoms are distributed uniformly in their crystals (Fig. S12†). The atomic ratio of P, Ag and Zr elements is almost consistent with the theoretical results (obtained from single-crystal structure data), which indicates the high purity of the sample. The phase purities of these crystals were also proved by their powder XRD patterns (Fig. S15 and S16†). Although **PTC-374(*S*,Λ)** is based on a supramolecular stacking framework, it can be stable in air, H_2O and some common organic solvents (such as MeOH, EtOH, THF, MeCN, *etc.*), as demonstrated by PXRD (Fig. S17†). However, it can be soluble in DMF. Liquid-state CD measurements were carried out at room temperature on large amounts of **PTC-374(*R*,Δ)** and **PTC-374(*S*,Λ)** samples. As shown in Fig. 3a, their CD peaks reveal obvious mirror images, indicating their absolute configuration and enantiomeric nature. In addition, we chose about 18 different single crystals of **PTC-374(*R*,Δ)** or **PTC-374(*S*,Λ)** from the same reaction bottle and tested their CD properties (Fig. S20 and S21†). The results show that they exhibit similar CD signal peaks, which further demonstrate their complete separation. The CD peaks at around 390, 310, 280, and 260 nm are similar to those of spontaneously resolved PTC-102 (Δ) and PTC-102(Λ) with only ΔΔΔΔ-Zr_4L_6 and ΛΛΛΛ-Zr_4L_6 isomers in its chiral structure (Fig. 3b). Thus, the π–π* transition and exciton coupling of the naphthyl groups in the L ligand occur at 260 and 280 nm, which can also be demonstrated *via* the UV adsorption spectrum (Fig. S22†). The intense negative and positive exciton splitting patterns centered at 310 nm can be assigned to the π–π* transition of the phenol and carboxylic oxygen moieties, indicating that each Zr center in **PTC-374(*R*,Δ)** and **PTC-374(*S*,Λ)** is in the Δ and Λ configuration, respectively. The observed peak at 390 nm corresponds to the metal-to-ligand charge transfer (MLCT) transition. Compared to ΔΔΔΔ-Zr_4L_6 and ΛΛΛΛ-Zr_4L_6 cages, the CD spectra of **PTC-374(*R*,Δ)** and **PTC-374(*S*,Λ)** both display a clear peak at 345 nm (green dotted line), which is attributed to the phenyl π–π* transition of the chiral BINAP ligand, as demonstrated by its UV-Vis and CD spectra as well as its coordination cation (Fig. S18, S19, S23 and S24†). Apparently, co-assembled **PTC-374(*R*,Δ)** and **PTC-374(*S*,Λ)** show a synergistic CD response herein.

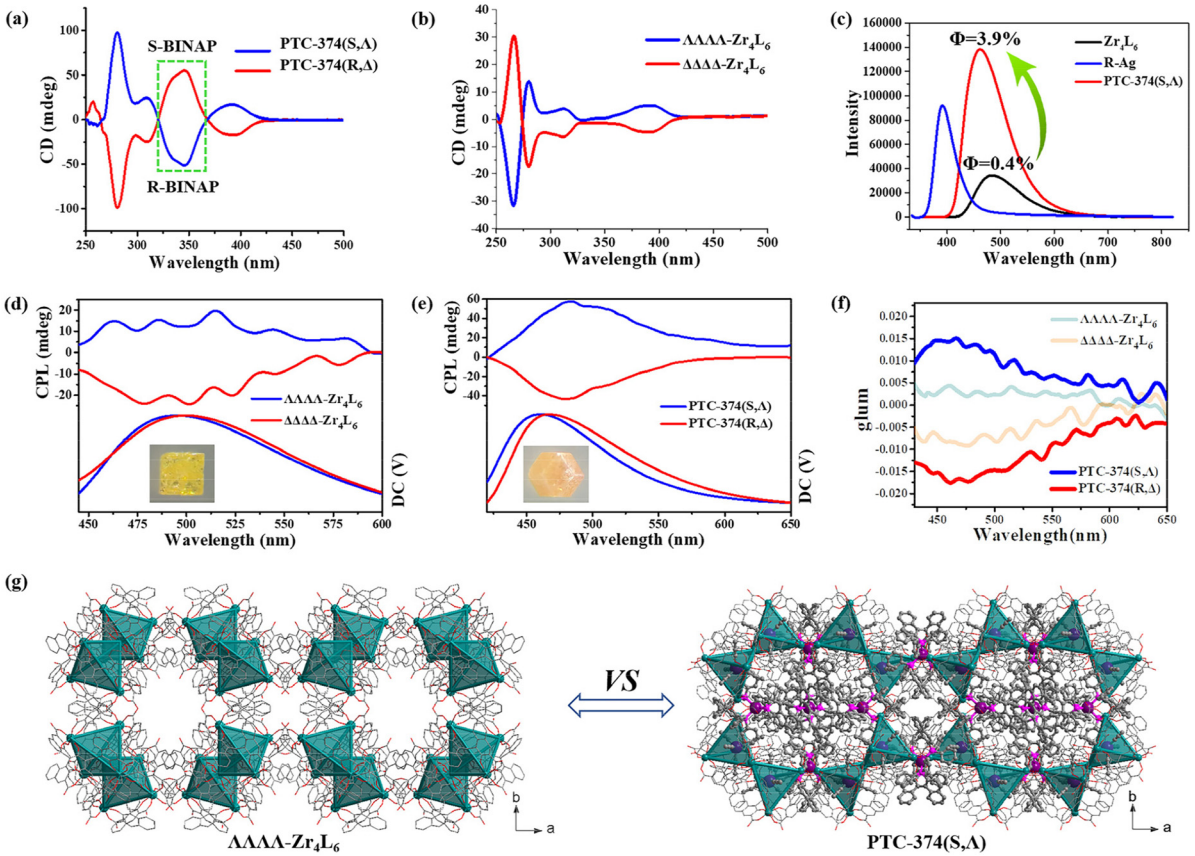

Fig. 3 (a) Liquid-state CD spectra of ΔΔΔΔ-Zr_4L_6 and ΛΛΛΛ-Zr_4L_6 cages in PTC-102(Δ) and PTC-102(Λ) single crystals (DMF solution), respectively; (b) liquid-state CD spectra of **PTC-374(*R*,Δ)** and **PTC-374(*S*,Λ)** in DMF; (c) luminescence spectra of Zr_4L_6, ***R*-Ag** and **PTC-374(*S*,Λ)** in the solid state; (d) CPL spectra of ΔΔΔΔ-Zr_4L_6 and ΛΛΛΛ-Zr_4L_6 cages (λ_{ex} = 340 nm); (e) CPL spectra of **PTC-374(*R*,Δ)** and **PTC-374(*S*,Λ)** (λ_{ex} = 370 nm); (f) dissymmetry factors (g_{lum}); (g) comparison of structures between PTC-102(Λ) and **PTC-374(*S*,Λ)**.

What effect does the combination of two chiral components have on the optical property? Firstly, we investigated the photoluminescence (PL) property of such a cooperatively self-assembled structure, and the solid-state emission spectra of Zr_4L_6 cage raw materials (PTC-102(Δ) and PTC-102(Λ)), ***R*-Ag** and **PTC-374(*S*,Λ)** were recorded in air at room temperature. ***R*-Ag** shows an emission maxima at 390 nm (λ_{ex} = 375 nm), which can be assigned to the phenyl π–π* transition of the chiral BINAP ligands, as also proved by the UV-Vis spectra of BINAP and its coordination cation (Fig. S23 and S24†). Upon excitation at 425 nm, the Zr_4L_6 cage displays an emission peak similar to that of the L ligands (Fig. 3c and S28†), and it has the highest emission peak at 480 nm in the 400–600 nm band, which may belong to the phenyl π–π* transition of the L ligands in the Zr_4L_6 cage. Under the same excitation wavelength and test conditions, the co-assembled structure **PTC-374(*S*,Λ)** shows an emission peak similar to Zr_4L_6 cages, and its emission peak can be observed at 460 nm. Their excitation spectra and PL photographs are shown in Fig. S27.† Remarkably, **PTC-374(*S*,Λ)** exhibits a stronger photoluminescence in comparison, and its emission intensity is about 4 times that of the Zr_4L_6 cage. In addition, it shows a slight blue-shift (*ca.* 20 nm) in comparison with the Zr_4L_6 cage. The absolute emission quantum yields (Φ) were also measured for the Zr_4L_6 cage and **PTC-374(*S*,Λ)** at room temperature upon excitation at 425 nm. It is calculated that the Φ value (*ca.* 3.9%) of **PTC-374(*S*,Λ)** is about 10 times than that of Zr_4L_6 (*ca.* 0.4%). Chiral *R*/*S*-BINAP ligands are highly conjugated organic ligands, and they readily coordinate with Ag^+ ions to form π-conjugated coordination Ag cations (***R*-Ag** and ***S*-Ag**). ***R*-Ag** or ***S*-Ag** has a strong photoluminescence property, which can be proved by its emission spectrum and fluorescence photograph (Fig. 3c and S27†). The combination of such luminescent Ag units and Ti_4L_6 cages into tightly packed and ordered structures significantly enhanced the PL performance, thus revealing a synergistic luminescence effect.

The synergistic CD effect and enhanced PL property encouraged us to further investigate the CPL performance of **PTC-374(*R*,Δ)** and **PTC-374(*S*,Λ)**. Due to the existence of the two racemic PTC-102(Δ) (only ΔΔΔΔ-Zr_4L_6 cages) and PTC-102(Λ) (only ΛΛΛΛ-Zr_4L_6 cages) structures in the single crystals, the single-crystal CPL was measured for convenience of comparison. In fact, such a test method has been reported.[31–33] Tactfully, PTC-102(Δ) (or PTC-102(Λ)) and **PTC-374(*R*,Δ)** (or **PTC-374(*S*,Λ)**) are all regular crystals. In order to eliminate differences due to factors such as angle and size, we chose

same-size crystals for testing, and tested the same single crystal (100) plane (Fig. 3d and e). The degree of CPL can be evaluated using the dissymmetry factors (g_{lum}), which is defined as $g_{lum} = 2(I_L - I_R)/(I_L + I_R)$, where I_L and I_R represent the luminescence intensities of left- and right-handed polarized light, respectively. As shown in Fig. 3e and f, single-crystal **PTC-374(*R*,Δ)** shows remarkable CPL in the visible region with a negative g_{lum} value of -1.75×10^{-2} at 465 nm, while **PTC-374 (*S*,Λ)** shows a mirror-image spectrum with a positive g_{lum} value of $+1.50 \times 10^{-2}$ at 465 nm. However, the CPL extremes of PTC-102(Δ) and PTC-102(Λ) single crystals can be observed at 465 nm with the g_{lum} values of -4.2×10^{-3} and 8.5×10^{-3}, respectively. Prominently, the g_{lum} values of **PTC-374** enantiomers in the excited state were boosted by an order of magnitude. Comparing the structure of PTC-102(Λ) and **PTC-374 (*S*,Λ)**, we found that they have the same chiral space group of *I*23 (Fig. 3g) and the ΛΛΛΛ-Zr_4L_6 cages in their structures have similar spatial arrangement, although their compositions and synthesis methods are vastly different. The only difference is that there are chiral $[Ag(S\text{-BINAP})_2]^+$ units in **PTC-374(*S*,Λ)**, thus resulting in larger cell parameters. In addition, there are no obvious supramolecular interactions between adjacent ΛΛΛΛ-Zr_4L_6 cages in PTC-102(Λ), while the opposite is true for **PTC-374(*S*,Λ)**. We preliminarily speculate that the introduction of chiral luminescence through Ag units and the abundant H-bonding interactions between adjacent lattice units (ΛΛΛΛ-Zr_4L_6 and $[Ag(S\text{-BINAP})_2]^+$) effectively increases the rigidity of the supramolecular frameworks, which realizes chiral synergistic amplification and fluorescence enhancement, so as to boost the CPL performance of the co-assembled material **PTC-374(*S*,Λ)**.

4. Conclusions

In summary, we realized the chiral resolution and functional application of a tetrahedral $Zr_4(embonate)_6$ cage. Through suitable supramolecular interactions, anionic ΔΔΔΔ-Zr_4L_6 and ΛΛΛΛ-Zr_4L_6 cages have been successfully resolved by enantiopure $[Ag(R\text{-BINAP})_2]^+$ and $[Ag(S\text{-BINAP})_2]^+$ cations, respectively. Such an unusual resolution process is accompanied by the stepwise transfer of homochirality, leading to chiral amplification from an enantiopure molecule to a final homochiral supramolecular framework with zeolitic SOD topology. Interestingly, the perfect combination of chiral zirconium cages and luminescent Ag units showed synergistic CD, enhanced fluorescence and CPL output with g_{lum} values of $\sim 1.5 \times 10^{-2}$. These results indicate the potential application of such homochiral cages in the CPL field.

Author contributions

Conceptualization by J. Zhang. Funding acquisition by Y.-P. He and J. Zhang. Y.-P. He and J. Zhang wrote the manuscript. X. Meng synthesized the compounds and conducted the associated basic characterization studies. X. Meng and Q.-R. Ding characterized the CD/CPL properties of these compounds. All authors discussed the progress of the research and reviewed the manuscript.

Data availability

The data supporting this article have been included as part of the ESI.†

Conflicts of interest

There is no conflict of interest to report.

Acknowledgements

This work was supported by the National Natural Science Foundation of China (92261108 and 21935010) and the STS Project of Fujian-CAS (2023T3054).

References

1 L. A. Hall, D. M. D'Alessandro and G. Lakhwani, Chiral metal–organic frameworks for photonics, *Chem. Soc. Rev.*, 2023, **52**, 3567–3590.
2 X.-Y. Luo and M. Pan, Metal-organic materials with circularly polarized luminescence, *Coord. Chem. Rev.*, 2022, **468**, 214640.
3 Y.-T. Sang, J.-L. Han, T.-H. Zhao, P.-F. Duan and M.-H. Liu, Circularly Polarized Luminescence in Nanoassemblies: Generation, Amplification, and Application, *Adv. Mater.*, 2020, **32**, 1900110.
4 C. Zhang, S. Li, X.-Y. Dong and S.-Q. Zang, Circularly polarized luminescence of agglomerate emitters, *Aggregate*, 2021, **2**, e48.
5 J.-X. Gao, W.-Y. Zhang, Z.-G. Wu, Y.-X. Zheng and D.-W. Fu, Enantiomorphic Perovskite Ferroelectrics with Circularly Polarized Luminescence, *J. Am. Chem. Soc.*, 2020, **142**, 4756–4761.
6 Q.-F. Gu, J.-J. Zha, C.-L. Chen, X. Wang, W.-Y. Yao, J.-H. Liu, F.-Y. Kang, J.-L. Yang, Y.-Y. Li, D.-Y. Lei, Z.-Y. Tang, Y. Han, C.-L. Tan and Q.-C. Zhang, Constructing Chiral Covalent–Organic Frameworks for Circularly Polarized Light Detection, *Adv. Mater.*, 2023, **36**, 2306414.
7 H.-X. Huang, N.-Q. Li, W.-D. Li, X.-C. Mo, X.-S. Cao, J.-S. Miao, X.-J. Yin and C.-L. Yang, Synergistic Modulation of Excited State Ingredients and Chiroptical Activity for High–Performance Pure–Green Circularly Polarized Electroluminescence, *Adv. Funct. Mater.*, 2024, 2403191.
8 L. Shi, L.-Y. Zhu, J. Guo, L.-J. Zhang, Y.-A. Shi, Y. Zhang, K. Hou, Y.-L. Zheng, Y.-F. Zhu, J.-W. Lv, S.-Q. Liu and Z.-Y. Tang, Self–Assembly of Chiral Gold Clusters into

Crystalline Nanocubes of Exceptional Optical Activity, *Angew. Chem., Int. Ed.*, 2017, **56**, 15397–15401.

9 J. Tang, S.-Q. Zhang, B.-W. Zhou, W. Wang and L. Zhao, Hyperconjugative Aromaticity-Based Circularly Polarized Luminescence Enhancement in Polyaurated Heterocycles, *J. Am. Chem. Soc.*, 2023, **145**, 23442–23451.

10 O. G. Willis, F. Zinna and L. Di Bari, NIR–Circularly Polarized Luminescence from Chiral Complexes of Lanthanides and d–Metals, *Angew. Chem., Int. Ed.*, 2023, **62**, e202302358.

11 M.-X. Yu, C.-P. Liu, Y.-F. Zhao, S.-C. Li, Y.-L. Yu, J.-Q. Lv, L. Chen, F.-L. Jiang and M.-C. Hong, White–Light Emission and Circularly Polarized Luminescence from a Chiral Copper(I) Coordination Polymer through Symmetry–Breaking Crystallization, *Angew. Chem., Int. Ed.*, 2022, **61**, e202201590.

12 J. Zhou, X.-F. Yang, P.-S. Zheng, Q.-Z. Li, X.-W. Li, J.-S. Chai, B.-Y. Huang, S. Yang and M.-Z. Zhu, Construction of an $Au_{12}Cd_2$ nanocluster with circularly polarized luminescence by a metal-and ligand-exchange strategy, *Chem. Sci.*, 2024, **15**, 4853–4859.

13 J.-G. Yang, K. Li, J. Wang, S.-S. Sun, W.-J. Chi, C. Wang, X.-Y. Chang, C. Zou, W.-P. To, M.-D. Li, X.-G. Liu, W. Lu, H.-X. Zhang, C.-M. Che and Y. Chen, Controlling Metallophilic Interactions in Chiral Gold(I) Double Salts towards Excitation Wavelength–Tunable Circularly Polarized Luminescence, *Angew. Chem., Int. Ed.*, 2020, **59**, 6915–6922.

14 X.-H. Tang, H. Jiang, Y.-B. Si, N. Rampal, W. Gong, C. Cheng, X. Kang, D. Fairen-Jimenez, Y. Cui and Y. Liu, Endohedral functionalization of chiral metal-organic cages for encapsulating achiral dyes to induce circularly polarized luminescence, *Chem*, 2021, **7**, 2771–2786.

15 Z.-Q. Li, Y.-D. Wang, J.-Y. Shao, Z.-Y. Zhou, Z.-L. Gong, C. Zhang, J.-N. Yao and Y.-W. Zhong, Electrically Amplified Circularly Polarized Luminescence by a Chiral Anion Strategy, *Angew. Chem., Int. Ed.*, 2023, **62**, e202302160.

16 J.-Y. Wang, Y.-B. Si, X.-M. Luo, Z.-Y. Wang, X.-Y. Dong, P. Luo, C. Zhang, C.-Y. Duan and S.-Q. Zang, Stepwise Amplification of Circularly Polarized Luminescence in Chiral Metal Cluster Ensembles, *Adv. Sci.*, 2023, **10**, 2207660.

17 X.-Z. Wang, C.-W. Zhou, J. Zheng, Z.-X. Lian, M.-Y. Sun, Y.-L. Huang, D. Luo, Y.-Y. Li and X.-P. Zhou, Highly Boosting Circularly Polarized Luminescence of Chiral Metal–Imidazolate Frameworks, *Adv. Sci.*, 2023, **10**, 2207333.

18 G. Zhang, Y.-L. Bao, H.-T. Ma, N.-W. Wang, X.-X. Cheng, Z.-X. He, X. Wang, T.-F. Miao and W. Zhang, Precise Modulation of Circularly Polarized Luminescence via Polymer Chiral Co–assembly and Contactless Dynamic Chiral Communication, *Angew. Chem., Int. Ed.*, 2024, **63**, e202401077.

19 G. Soldan, M. A. Aljuhani, M. S. Bootharaju, L. G. AbdulHalim, M. R. Parida, A. H. Emwas, O. F. Mohammed and O. M. Bakr, Gold Doping of Silver Nanoclusters: A 26-Fold Enhancement in the Luminescence Quantum Yield, *Angew. Chem., Int. Ed.*, 2016, **55**, 5749–5753.

20 Y. Wu, L.-H. You, Z.-Q. Yu, J.-H. Wang, Z.-G. Meng, Y. Liu, X.-S. Li, K. Fu, X.-K. Ren and B.-Z. Tang, Rational Design of Circularly Polarized Luminescent Aggregation-Induced Emission Luminogens (AIEgens): Promoting the Dissymmetry Factor and Emission Efficiency Synchronously, *ACS Mater. Lett.*, 2020, **2**, 505–510.

21 Y.-P. He, L.-B. Yuan, G.-H. Chen, Q.-P. Lin, F. Wang, L. Zhang and J. Zhang, Water-Soluble and Ultrastable Ti_4L_6 Tetrahedron with Coordination Assembly Function, *J. Am. Chem. Soc.*, 2017, **139**, 16845–16851.

22 G.-H. Chen, Y.-P. He, Z.-R. Wang, Q.-H. Li, Z.-Z. Ma and J. Zhang, Tunable third-order nonlinear optical effect via modifying Ti_4(embonate)$_6$ cage-based ionic pairs, *Inorg. Chem. Front.*, 2022, **9**, 1984–1991.

23 G.-H. Chen, Y.-P. He, Y.-H. Yu, Q.-H. Li and J. Zhang, Homochiral design of titanium-organic cage for circularly polarized luminescence-based molecular detection, *Sci. China: Chem.*, 2023, **66**, 2558–2562.

24 G.-H. Chen, Y.-P. He, Y.-H. Yu, H. Lv, S.-D. Li, F. Wang, Z.-G. Gu and J. Zhang, Post–Assembly Modification of Homochiral Titanium–Organic Cages for Recognition and Separation of Molecular Isomers, *Angew. Chem., Int. Ed.*, 2023, **62**, e202300726.

25 R.-Y. Chen, Y.-P. He, G.-H. Chen and J. Zhang, Designing Cage-Supported Cluster-Organic Framework for Highly Efficient Optical Limiting, *ACS Mater. Lett.*, 2022, **4**, 1397–1401.

26 Y.-P. He, G.-H. Chen, D.-J. Li, Q.-H. Li, L. Zhang and J. Zhang, Combining a Titanium–Organic Cage and a Hydrogen–Bonded Organic Cage for Highly Effective Third–Order Nonlinear Optics, *Angew. Chem., Int. Ed.*, 2020, **60**, 2920–2923.

27 Y.-F. Li, Y.-P. He, Q.-H. Li and J. Zhang, Integrated Anionic Zirconium–Organic Cage and Cationic Boron–Imidazolate Cage for Synergetic Optical Limiting, *Angew. Chem., Int. Ed.*, 2024, **63**, e202318806.

28 Q. Teng, Y.-P. He, G.-H. Chen and S.-M. Chen, Cage–Ligand Strategy for the Construction of Zr_4(embonate)$_6$-Based MOFs with Third–Order Nonlinear–Optical Properties, *Chin. J. Chem.*, 2022, **40**, 2067–2071.

29 G.-H. Chen, H.-Z. Li, Y.-P. He, S.-H. Zhang, X.-F. Yi, F.-P. Liang, L. Zhang and J. Zhang, Ti_4(embonate)$_6$ Based Cage-Cluster Construction in a Stable Metal–Organic Framework for Gas Sorption and Separation, *Cryst. Growth Des.*, 2019, **20**, 29–32.

30 Y.-P. He, L.-B. Yuan, J.-S. Song, G.-H. Chen, Q.-P. Lin, C.-S. Li, L. Zhang and J. Zhang, Optical Resolution of the Water-Soluble Ti_4(embonate)$_6$ Cages for Enantioselective Recognition of Chiral Drugs, *Chem. Mater.*, 2018, **30**, 7769–7775.

31 M. Hu, F.-Y. Ye, C. Du, W.-Z. Wang, T.-T. Zhou, M.-L. Gao, M.-H. Liu and Y.-S. Zheng, Tunable Circularly Polarized Luminescence from Single Crystal and Powder of the Simplest Tetraphenylethylene Helicate, *ACS Nano*, 2021, **15**, 16673–16682.

32 O. Oki, C. Kulkarni, H. Yamagishi, S. C. J. Meskers, Z. H. Lin, J. S. Huang, E. W. Meijer and Y. Yamamoto, Robust Angular Anisotropy of Circularly Polarized Luminescence from a Single Twisted-Bipolar Polymeric Microsphere, *J. Am. Chem. Soc.*, 2021, **143**, 8772–8779.

33 J. Zhao, T.-J. Zhang, X.-Y. Dong, M.-E. Sun, C. Zhang, X.-L. Li, Y.-S. Zhao and S.-Q. Zang, Circularly Polarized Luminescence from Achiral Single Crystals of Hybrid Manganese Halides, *J. Am. Chem. Soc.*, 2019, **141**, 15755–15760.